ADVANCED ENERGY MATERIALS
www.advenergymat.de

An Anion-Tuned Solid Electrolyte Interphase with Fast Ion Transfer Kinetics for Stable Lithium Anodes

*Zhenxing Wang, Fulai Qi, Lichang Yin, Ying Shi, Chengguo Sun, Baigang An, Hui-Ming Cheng, and Feng Li**

The spatial distribution and transport characteristics of lithium ions (Li^+) in the electrochemical interface region of a lithium anode in a lithium ion battery directly determine Li^+ deposition behavior. The regulation of the Li^+ solvation sheath on the solid electrolyte interphase (SEI) by electrolyte chemistry is key but challenging. Here, 1 M lithium trifluoroacetate (LiTFA) is induced to the electrolyte to regulate the Li^+ solvation sheath, which significantly suppresses Li dendrite formation and enables a high Coulombic efficiency of 98.8% over 500 cycles. With its strong coordination between the carbonyl groups (C=O) and Li^+, TFA^- modulates the environment of the Li^+ solvation sheath and facilitates fast desolvation kinetics. In addition, due to relatively smaller lowest unoccupied molecular orbital energy than solvents, TFA^- has a preferential reduction to produce a stable SEI with uniform distribution of LiF and Li_2O. Such stable SEI effectively reduces the energy barrier for Li^+ diffusion, contributing to low nucleation overpotential, fast ion transfer kinetics, and uniform Li^+ deposition with high cycling stability. This work provides an alternative insight into the design of interface chemistry in terms of regulating anions in the Li^+ solvation sheath. It is anticipated that this anion-tuned strategy will pave the way to construct stable SEIs for other battery systems.

Metallic lithium (Li), with a high specific capacity (3860 mAh g^{-1}) and the lowest redox potential (−3.04 V vs standard hydrogen electrode), has been considered as the most promising anode candidate for high-energy rechargeable batteries.[1] However, the uncontrolled dendrite formation and poor reversible Li plating/stripping efficiency long hinder its practical application. Fundamentally, the reactive nature of Li metal can spontaneously trigger side reactions with the electrolyte and form a passivation layer (called solid electrolyte interphase, SEI).[2] The chemical heterogeneity and mechanical instability of SEI are generally considered as the reasons for dendrite formation.[3] Therefore, manipulating the electrolyte chemistry is considered as the most effective method, for it can directly impact the properties of SEI and alter Li^+ deposition behavior.[4]

In the electrolyte, Li^+ is solvated by solvents and anions to form the Li^+ solvation sheath.[5] The Li^+ solvation sheath can diffuse freely in bulk electrolyte, which has a higher probability of reaching Li surface. Once reaching Li metal surface, the solvent molecules and anions from the solvation sheath will be reduced by electrons and compose the main components of SEI, thereby modulating Li^+ transport and deposition behavior.[6] Due to the diverse reactivity and proportion in the Li^+ solvation sheath, the components from solvents and anions at the interface chemistry are distinctly different.[7] For the dilute electrolytes (ethers and ethers), more solvent molecules dominated the Li^+ solvation sheath due to high ratios of solvent/anions (e.g., 11.6:1 in 1 M lithium hexafluorophosphate ($LiPF_6$)-ethylene carbonate (EC)/diethyl carbonate (DEC)). The reduction species in the SEI depend on the reactivity and proportion of the components (solvents and anions) in the Li^+ solvation sheath.[8] With a high proportion of solvent molecules in the solvation sheath, the as-obtained SEI as principally composed of solvent-derived organic species (ROLi, RCOOLi, and $ROCO_2Li$), accompanied by few inorganic species (LiF, Li_2S, and Li_2O) mainly originating from anions.[4a,9] Such solvent-derived SEI with highly resistive nature can bring about sluggish transport and uneven charge distribution of Li^+, resulting in notorious dendrite growth and low Coulombic efficiency (CE, 80%).[10] Inducing F atoms into the molecular structure of solvents can increase the reactivity of the Li^+ solvation sheath.[11] For instance, fluoroethylene carbonate (FEC) has a relatively smaller lowest unoccupied molecular orbital (LUMO) than EC, which can be preferentially reduced to form a SEI

Z. Wang, Dr. F. Qi, Prof. L. Yin, Y. Shi, Prof. H.-M. Cheng, Prof. F. Li
Shenyang National Laboratory for Materials Science
Institute of Metal Research
Chinese Academy of Sciences
72 Wenhua Road, Shenyang 110016, China
E-mail: fli@imr.ac.cn

Z. Wang, Dr. F. Qi, Y. Shi, Prof. F. Li
School of Materials Science and Engineering
University of Science and Technology of China
Hefei 230026, China

Prof. C. Sun, Prof. B. An
School of Chemical Engineering
University of Science and Technology Liaoning
Anshan 114051, China

Prof. H.-M. Cheng
Shenzhen Geim Graphene Center
Tsinghua-Berkeley Shenzhen Institute
Tsinghua University
Shenzhen 518055, China

The ORCID identification number(s) for the author(s) of this article can be found under https://doi.org/10.1002/aenm.201903843.

DOI: 10.1002/aenm.201903843

high proportion of LiF. The SEI can enhance the interfacial transport of Li^+ and enable higher CE (90%).[12] Employing aromatic fluorinated groups (CF_3) on the solvent molecules can adjust the LUMO energy of a SEI layer for stabilizing the Li metal anodes.[11] However, the CE performance is still deficient for practical applications of Li metal anodes. In addition, highly concentrated electrolytes have also been demonstrated to modulate Li^+ solvation sheath for stable Li anode with high CE.[9,13] Despite the decreased solvent/salt ratio (almost 1:1 in highly concentrated electrolytes), more anions take in the Li^+ solvation sheath and produce a SEI layer with a greater amount of inorganic components, resulting in uniform Li^+ transport with fast kinetics. Of course, highly concentrated electrolytes will raise the cost and bring about high electrolyte viscosity which makes it hard for the practical application of Li metal anodes.[14] Recently, the reports have emphasized the importance of regulating the anions for stable Li metal anodes, such as enriching the Li^+ solvation sheath by inducing NO_3^- anions and modulating the inner Helmholtz plane with the introduction of NO_3^-/F^- anions.[5,15] Therefore, developing new types of anions is highly desirable for constructing ideal SEI with modulated Li^+ deposition. A desired Li salt should have a good dissociation in aprotic solvents and produce stable SEI protecting Li metal. Introduction of electron-withdrawing groups into anions, especially electronegative F atoms, can promote easy dissociation because of weak coordination ability between anions and cations.[16] Additionally, the electronegative F atom can adjust the frontier molecular orbitals for benefiting the stability of SEI.[11] To regulate the environment of Li^+ solvation sheath, anions with carbonyl group (C=O) or carboxyl group (COO^-) are better choice for their strong coordination with Li^+.[17]

Here, an electrolyte based on 1 M lithium trifluoroacetate (LiTFA) in 1, 2-dimethoxyethane (DME)/FEC enables a high CE of 98.8% over 500 cycles. With strong coordination between carbonyl group (C=O) and Li^+, TFA^- can modulate the environment of Li^+ solvation sheath and facilitate fast desolvation kinetics. During SEI formation, TFA^- has a preferential reduction than solvents for the lower LUMO energy, contributing to an abundance of LiF and Li_2O. Such stable SEI renders long cleavage of epoxy and fast ion transfer kinetics by reducing the energy barrier when Li^+ diffuses through SEI. Therefore, uniform Li^+ deposition with spherical morphologies is achieved. Coupled with lithium iron phosphate (LFP) and aggressive $LiNi_{0.6}Co_{0.2}Mn_{0.2}O_2$ (NCM622) cathodes, the full cells with limited Li at the anode enabled longer cycling stability than the control samples.

Based on frontier molecular orbital theory, the components of SEI highly depend on the LUMO of the solute or solvents in the electrolyte. Inspired for this, the molecular orbital energy of LiTFA was calculated by density functional theory (DFT) to explore its thermodynamic potential of forming a new interface. **Figure 1** shows the energy levels of LUMO and highest occupied molecular orbital (HOMO) of the solute and solvents. The reduction potential decreased in the following order: LiTFA > $LiPF_6$ > FEC > EC > DEC > DME, indicating that LiTFA has a higher tendency to be reduced during SEI formation. Here, 1 M LiTFA was induced into DME/FEC to evaluate its performance. DME was chosen as the solvent for its low reaction activity with Li (LUMO: 2.30 eV). To enhance the oxidation ability of DME

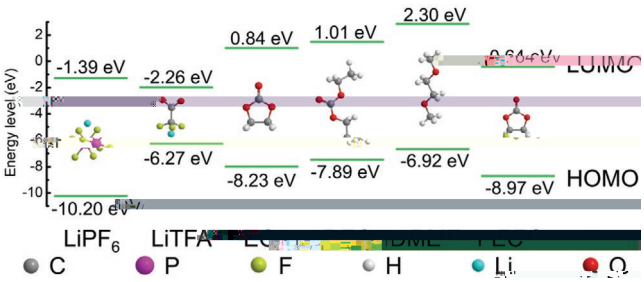

Figure 1. Molecular orbital energies of solutes and solvents. The data for the solvents (e.g., EC, DEC, DME, and FEC) are taken from two previous reports.[19]

(oxidation potential less than 4.0 V vs Li^+/Li) for the application in high-voltage cathodes,[5,18] FEC (HOMO: –8.97 eV) was selected as the corporative solvent.

To investigate Li^+ plating/stripping behavior, the CE in the different electrolytes was evaluated by Li||C cells. In 1 M $LiPF_6$-EC/DEC, the initial CE was only 85% and subsequently showed a fast decay at 0.5 mA cm^{-2} (**Figure 2**a). In this electrolyte, more solvent molecules dominated the Li^+ solvation sheath and resulted in a SEI principally composed of solvent derived organic species ($ROCO_2Li$), as well as little LiF produced by decomposition of PF_6^-.[4a] Such solvent derived SEI as decay consistently a stable SEI for protecting Li anode, thereby leading to poor Li plating/stripping efficiency. With a lower LUMO energy than EC (0.84 eV), FEC (–0.64 eV) has a higher potential to preferentially decompose and regulate the SEI with more LiF.[20] DME has a lower reactivity with Li metal for its higher LUMO energy (2.30 eV) than carbonates. After replacing EC/DEC with DME/FEC, the volume expansion of the CE just retained to 90%. Even replacing $LiPF_6$ with salt lithium bis(trifluoromethanesulfonyl)imide (LiTFSI), the CE and cycling stability were still not improved with a significant increase (Figure S1, Supporting Information). With lower energy of LUMO (–2.26 eV), LiTFA was introduced to DME/FEC for regulating the reactivity of Li^+ solvation sheath. As Figure S2, Supporting Information shows, although with a moderate ionic conductivity (5.4 mS cm^{-1}), 1 M LiTFA-DME/FEC achieved a significantly higher CE of 95.5% for the initial cycle and gradually ramped up to ≈98.8% after 130 cycles. After increasing the higher current density and higher areal capacity (Figure S3, Supporting Information), the average CE in LiTFA-DME/FEC still exhibited higher Li plating/stripping CE than $LiPF_6$-EC/DEC and $LiPF_6$-DME/FEC electrolytes. To eliminate the effect of DME and FEC on the CE performance, we added the CE testing at 0.5 mA cm^{-2} first, fixed 1 mAh cm^{-2} in other different electrolytes. As shown in Figure S4, Supporting Information, the electrolyte of 1 M LiTFA-DME enables higher CE than other electrolytes, indicating that LiTFA plays a critical role on improving the cycling stability of Li metal anode. The interactions among Li^+, anions and solvent molecules were investigated by attenuated total reflection Fourier transform infrared (ATR-FTIR) from 1 cm^{-1} resolution. The spectra of LiTFA-DME/FEC electrolyte as depicted in Figure 2b, the emerging characteristic bands at 720 and 1065 cm^{-1} can be assigned as the aggregates of Li^+ solvation sheath.[21] Notably, the C=O asymmetric stretching frequency of LiTFA exhibited

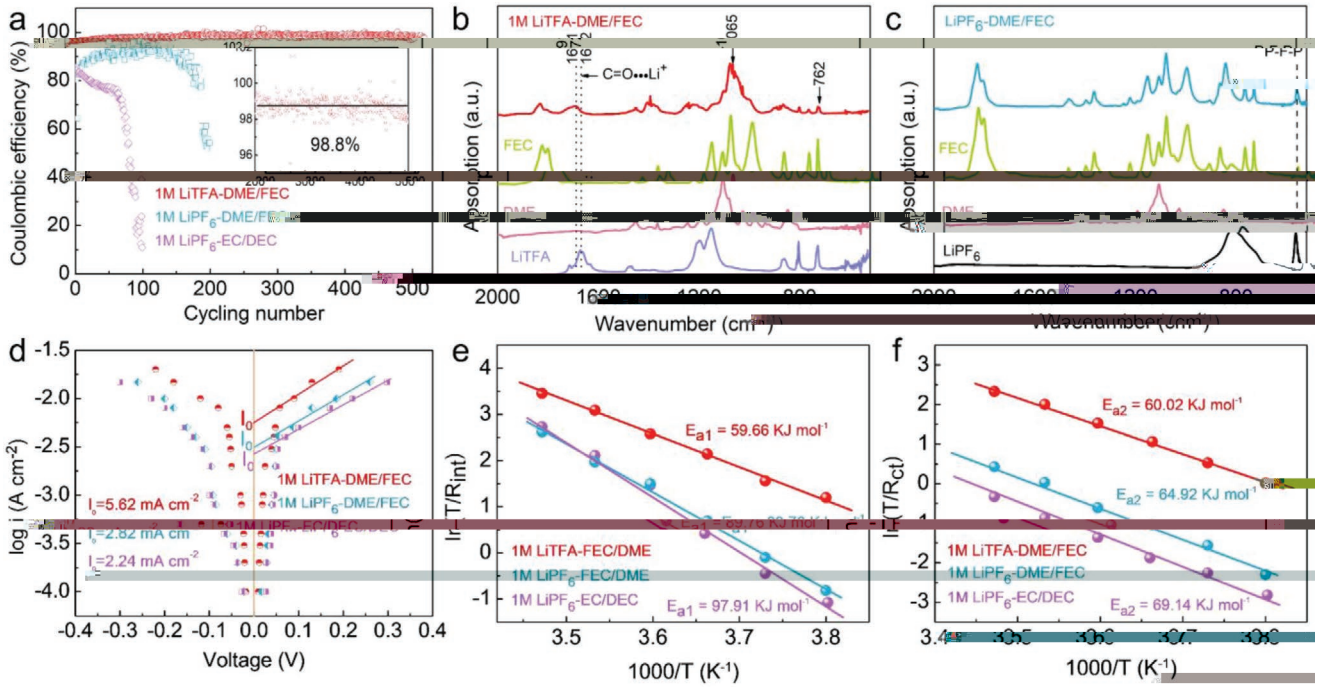

Figure 2. Electrochemical performance in different electrolytes. a) Li plating/stripping efficiency on a Cu working electrode in different electrolytes at a current density of 0.5 mA cm^{-2} with a fixed capacity of 1.0 mAh cm^{-2}. b) ATR-FTIR spectra of LiTFA, DME, FEC, and 1 M LiTFA-DME/FEC. c) ATR-FTIR spectra of $LiPF_6$, DME, FEC, and 1 M $LiPF_6$-DME/FEC. d) Tafel plots for Li plating/stripping in different electrolytes. The Tafel plot was obtained by plotting the overpotential of galvanostatic Li plating/stripping to the natural log of the current density. e) and f) The activation energies of R_{int} and R_{ct} derived from Nyquist plots.

ong bl e hif (19 cm^{-1}), hich indica d ong in ra ion be een Li$^+$ and carbon l o gen gro p in he Li$^+$ ol a ion hea h.[17,21] In con a for $LiPF_6$-EC/DEC and $LiPF_6$-DME/FEC, he pical chara ri ic PF_6^- peak a 562 cm^{-1} (P-F-P) a almo he ame a he ndi ol ed a indica ing minimal anion pa ip a ing in he Li$^+$ ol a ion hea h (Fig re S5, S pp ing Informa ion and Fig re 2c).[22] Therefore, he high CE and long c cling bili erif a TFA^- ake in he Li$^+$ ol a ion hea h and b eq en reg la e he prope ie of SEI minimi e ide reac ion a Li/elec ol in er face.

In order nder and he proce he elec ode kine ic in differen elec ol ere in e ga d. A ho n in Fig re S6a, S pp ing Informa ion, he o erpo en ial of ini ial Li$^+$ pla ing/ pping in $LiPF_6$-EC/DEC a 38 mV, b increa ed 58 mV (50) and 115 mV (100). The large o erpo en ial a ari ed from he highl re i e SEI prod ced b e ere ide reac ion a Li/elec ol in er face, hich increa ed he ion an por re i ance.[20] The polari a ion a igni red in $LiPF_6$-DME/FEC (1 34 mV, 50 : 47mV, and 100 : 95 mV) d e lo reac ion be een Li and DME (Fig re S6b, S pp ing Informa ion). While af r replacing PF_6^- TFA^- (Fig re S6c, S pp ing Information), he o erpo en ial a grea red (150 : 88 mV). To f her e al a he elec ochemical c cling bili of Li me al in differen elec ol he Li||Li mme ic cell ere in e ga d (Fig re S7, S pp ing Informa ion). i can be een ha he o erpo en ial of Li||Li cell in LiTFA-DME/FEC elec ol remain a lo er o erpo en ial a 2 mA cm^{-2} for more han 320 h, in con a he higher o erpo en ial in he $LiPF_6$-EC/DEC or $LiPF_6$-DME/FEC elec ol Thi re i gge ed ha TFA^- prod ced a cond c e SEI for lo er an-po ing re i ance d ring Li$^+$ pla ing/ pping. Li||Li mme ic cell ere f her a embled b gal ano c cling a ario c rren len e plore ion an fer kine ic a he in er face (Fig re 2d). The fa e change c rren len in LiTFA-DME/FEC a almo o me larger han ha in $LiPF_6$-EC/DEC (2.24 mA cm^{-2}) and $LiPF_6$-DME/FEC (2.82 mA cm^{-2}), indica ing fa ion an fer kine ic d ring Li$^+$ depo i on.[23] The Li$^+$ depo i on proce co ld be di ided in o fo r pa diff ion of ol a d Li$^+$ in b lk elec ol , Li$^+$ de ol a ion a SEI/elec ol in er face, Li$^+$ diff ion ro gh SEI, and Li$^+$ pla ing o er Li rface (Li$^+$ + e$^-$ = Li).[15,24] The Li$^+$ de ol a ion a SEI/elec ol in er face and Li$^+$ diff ion ro gh SEI la er are o ra e-de ermining ep here large energ barrier need o be o ercome.[25]

To mea re he ac a ion energ d ring Li$^+$ depo i on, he emperare-dependen elec ochemical impedance pec o cop (EIS) a carried o The a ob ained EIS pro le and he d eq i alen circ from 263 288 K ere ho n in Fig re S8 and Table S1 S3, S pp ing Informa ion. Ba ed on he Arrheni eq a ion:

$$k = \frac{T}{R_{re}} = A \exp\left(-\frac{E_a}{RT}\right) \quad (1)$$

here k repre en he ra con an T i he ab ol emperare, R_{re} i he ion an fer re i ance, A i he pre e ponen al con an E_a i he ac a ion energ , and R i he andard ga con an The ac a ion energ (E_a) i ob ained b ing he epara ed emicircle (R_{in} R_{ct}) in Li||Li mme ic

cell. (Figure 2e,f). R_{int} represents the resistance of Li^+ across the SEI at medium frequencies. R_{ct} represents the resistance of Li^+ desolvation at SEI/electrolyte interface at low frequencies (also denoted as charge transfer).[6b,26] The rate constant k is determined by T and the activation R_{int} or R_{ct} (Table S1–S3, Supporting Information). In accordance with the activation R_{int} and R_{ct}, the corresponding activation energy E_{a1} and E_{a2} are obtained by the Arrhenius equation. E_{a1}, representing the activation energy of Li^+ when passing through SEI, is reduced by more than 40% in LiTFA-DME/FEC (59.66 kJ mol^{-1}), compared with a larger energy barrier in $LiPF_6$-EC/DEC (97.91 kJ mol^{-1}) and $LiPF_6$-DME/FEC (89.76 kJ mol^{-1}) (Figure 2e). The decreased energy barrier proves that TFA^- in the Li^+ solvation sheath has a significant effect on the Li^+ transport kinetics of SEI. E_{a2} represents the energy barrier of Li^+ desolvation from Li^+ solvation sheath. Compared with Li^+ desolvation energy in $LiPF_6$-EC/DEC (69.14 kJ mol^{-1}) and $LiPF_6$-DME/FEC (64.92 kJ mol^{-1}), LiTFA-DME/FEC (60.02 kJ mol^{-1}) showed a slight decrease (Figure 2f). Generally, for aprotic polar solvent containing oxygen atoms, the coordination between Li^+ and solvent is far stronger than anion counterparts giving rise to higher Li^+ desolvation energy.[27] Supposed at 263 K, the R_{ct} and R_{int} for $LiPF_6$-EC/DEC, $LiPF_6$-DME/FEC, and LiTFA-DME/FEC are 4359, 2636, 260 Ω and 774, 598, 79 Ω, respectively. The corresponding k_{ct} and k_{int} are 0.060, 0.100, 1.012 and 0.400, 0.440, 3.330. Therefore, the strong coordination between C=O and Li^+, TFA^- can replace part of solvent molecules regulating the environment of Li^+ solvation sheath and facilitate fast ion transfer kinetics.

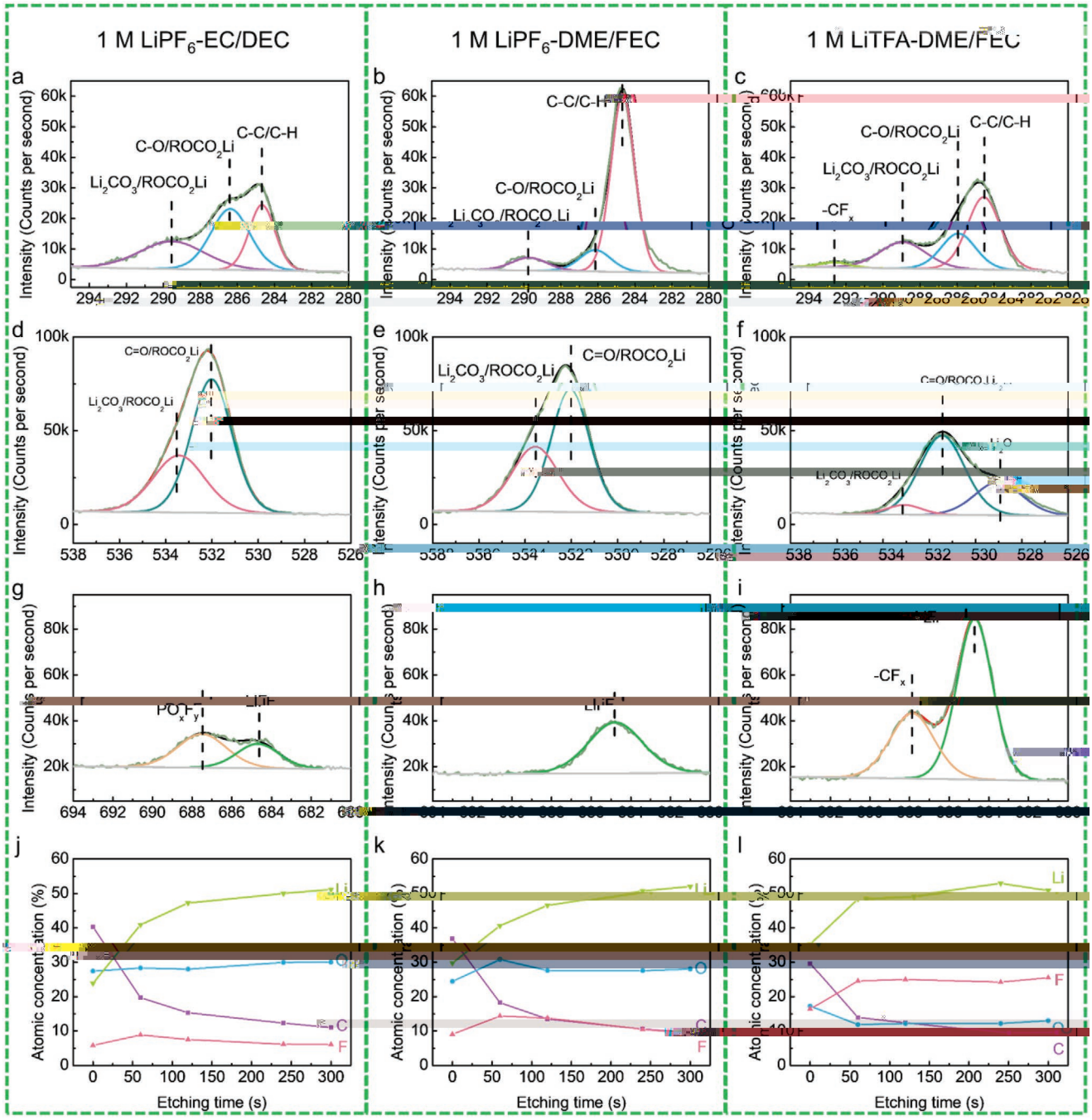

Figure 4. XPS characterization of the SEI components on cycled Li anodes in different electrolytes after 100 cycles. a), d), g), and j) are C1s, O1s, F1s spectra and atomic concentrations in the SEI of $LiPF_6$-EC/DEC; b), e), h), and k) are C1s, O1s, F1s spectra and atomic concentrations in the SEI of $LiPF_6$-DME/FEC; c), f), i), and l) are C1s, O1s, F1s spectra and atomic concentrations in the SEI of LiTFA-DME/FEC.

The chemical compo[illegible]ons of SEI on Li me[illegible] ere f [illegible]er e plored b X-ra pho[illegible]electron [illegible]pec[illegible]os[illegible]cop (XPS)[illegible] g re o[illegible] [illegible]he nderl ing mechani[illegible]m of di er[illegible]e ion[illegible]an[illegible]po[illegible]kine[illegible]s in differen[illegible]elec[illegible]ol[illegible]s (**Figure 4** and Fig re S9 S11, S pporting Informa[illegible]on). The [illegible]ignal[illegible] of C 1[illegible] [illegible]pec[illegible]a for [illegible]he [illegible]hree SEI lm[illegible] pre[illegible]en[illegible]d [illegible]imilar peak[illegible] corre[illegible]ponding [illegible] Li_2CO_3/$ROCO_2Li$, C-O/$ROCO_2Li$, and C C/C H cen[illegible]red a[illegible]289.5, 286.5, and 284.6 eV[28] (Fig re 4a c). The O 1[illegible] [illegible]pec[illegible]a (Fig re 4d f) ere [illegible]d in[illegible] Li_2CO_3/$ROCO_2Li$ (533.7 eV) and C=O/$ROCO_2Li$ (532.0 eV),[29] corre[illegible]ponding [illegible]o the decompo[illegible]on of [illegible]ol en[illegible]molec le[illegible] A[illegible] [illegible]p [illegible]ering [illegible]ne increa[illegible]ed, organic $ROCO_2Li$ al a[illegible] dominan[illegible] [illegible]he SEI of $LiPF_6$-EC/DEC and $LiPF_6$-DME/FEC ba[illegible]ed on peak area[illegible] a[illegible] ell a[illegible] [illegible]mall amo n[illegible]of inorganic Li_2O [illegible]ince 60 [illegible] re e[illegible]ng an ne en organic-domina[illegible]d la er (Fig re S10, S p-porting Informa[illegible]on). In[illegible]re[illegible]ngl , in SEI of LiTFA-DME/FEC, [illegible]able Li_2O a[illegible] de[illegible]ec[illegible]d from [illegible]op [illegible]o bo[illegible]om, [illegible]hich can be

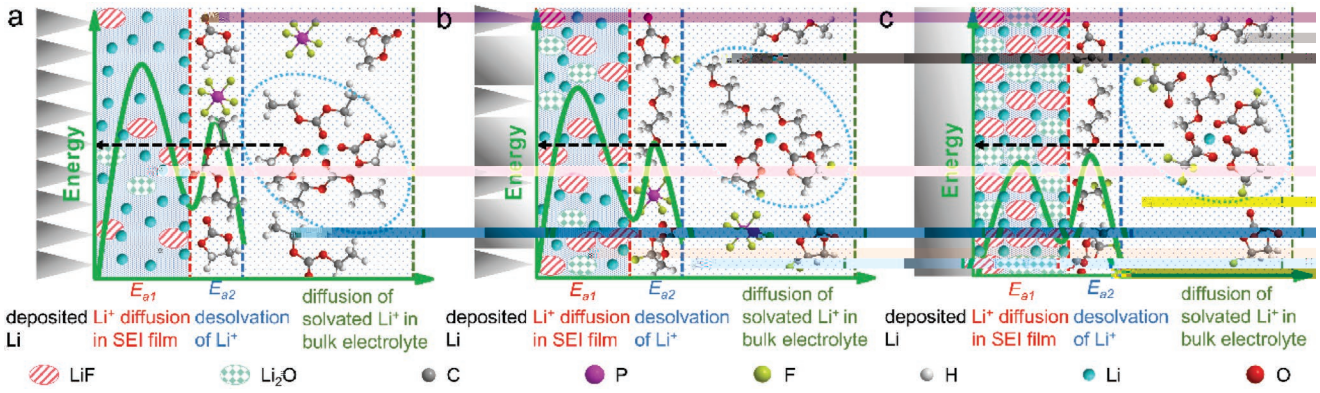

Figure 5. Schematics of the Li^+ deposition process in different electrolytes. a) $LiPF_6$-EC/DEC, b) $LiPF_6$-DME/FEC, and c) LiTFA-DME/FEC. The aggregates in the light-blue dotted ovals represent the Li^+ solvation sheath in the bulk electrolyte. The two bold dark-green waves correspond to the activation energies consumed on breakup of the Li^+ solvation sheath at the SEI/electrolyte interface (E_{a2}) and the diffusion of Li^+ through the SEI film (E_{a1}).

a×cribed a×%e decompo×i%ion of TFA⁻. In addi%ion, LiF (ari×ing from $LiPF_6$, FEC, or LiTFA) a× de%ec%ed a%≈684.6 eV[30] in all SEI lm× (Fig re 4g i). We al×o compared %e a%omic con%en% of elemen%al compo×i%on in differen%in%erface× (Fig re 4j l). Before Ar⁺ p %ering, %e SEI of LiTFA-DME/FEC ho ed a lo er a%omic con%en% of C (30%) and O (17%), in con%a% %e SEI of $LiPF_6$-EC/DEC (C: 41%, O: 27%) and $LiPF_6$-DME/FEC (C: 38%, O: 25%), implied a le× organic con%en% %e o %er la er. A× %e p %ering %me increa×ed, %e con%en% of C (organic pecie×) in all SEI lm× ho ed a rapid decline %in %e r %60 ×, b %O almo% kep% able. Thi× a× con×i%ed %e repor% %a% mo% organic pecie× ($ROCO_2Li$) co ered on %e o %er la er and par%al $ROCO_2Li$ ere hif%ed % inorganic prod c% (Li_2CO_3 and Li_2O) in %e inner la er.[31] In %e SEI of LiTFA-DME/FEC, inorganic Li_2O domina%d %e inner SEI ra%er %an organic $ROCO_2Li$ ince e%ching for 120 × (Fig re S10, S por%ing Infor%a%on). No%bl , %e a%omic con%en% of F (mainl LiF) in SEI of LiTFA-DME/FEC a× dra%ically increa×ed from 16% % 25% ince e%ching for 60 ×, hich kep% almo% %ree %me× higher %an %a% in LiPF6-EC/DEC (9%) and % o %me× higher %an in $LiPF_6$-DME/FEC (14%). The bond %eng% of TFA⁻ and PF_6^- ere f %er calc la%d % con rm %e difference. A× ho n in Fig re S12, S por%ing Information, %e bond %eng% of C F in TFA⁻ anion× (203.29 kJ mol^{-1}) a× remarkabl eaker %an %a% of P F in PF_6^- anion× (346.96 kJ mol^{-1}), × gge%ing %e bond-breaking po%en%al of prod cing a LiF-rich la er on Li me%l × rface. Therefore, TFA⁻ decompo×ed a %e dominan%ed c%on and prod ced a rob % SEI % an ab ndance of LiF and Li_2O, hich a× re×ponsible for lo ering %e energ barrier of Li^+ dif- f ×ion and con%ib %ing % fa% and niform Li^+ depo×i%on.

Ba×ed on %e repor% %e componen% of LiF and Li_2CO_3 ma al×o be deri ed from %e decompo×i%on× of FEC. The degrada%on mechani×m i× a× follo ×:[32]

$$FEC + Li^+ + e^- \rightarrow pol\ (VC) + LiF + Li_2CO_3 \quad (2)$$

In order % con rm %e o rce× of LiF and Li_2CO_3, XPS and × rface-enhanced Raman × %ering (SERS) ere cond c%d. LiF de%ec%d a% 684.6 eV in 1 M LiTFA-DME % FEC a× charac%ri ed (Fig re S13a, S por%ing Information). For O 1× pec% m (Fig re S13b, S por%ing Information), Li_2CO_3 de%ec%d a% 533.0 eV ma ari e e%er from LiTFA or DME ol en% To f %er e plore %e o rce of Li_2CO_3, 0.1 M LiTFA a× di×ol ed in CH_2Cl_2 ol en% (Fig re S14, S por%ing Information). Ob io l , no peak a× fo nd a% 1090 cm^{-1} (corre×ponding % Li_2CO_3[33]). Therefore, %e po×ible degrada- % proce×× of LiTFA i× a× follo ing:

$$C_2F_3O_2Li + nLi^+ + ne^- \rightarrow LiF + Li_2O + C_2F_2OLi_{n-2} \quad (3)$$

The red c%on po%en%al of LiTFA a× f %er e plored b c clic o%amme% (CV) in 1 M LiTFA-DME ing copper (C) elec%ode a% a canning ra% of 0.1 mV $×^{-1}$. A di%c%red c%on on e po%en%al a× fo nd a% abo % 1.1 V (× Li^+/Li) (Fig re S15, S por%ing Information). And no imilar red c%on peak can be ob er ed in %e DME ol en% % o % LiTFA. Therefore, %e ca%odic c rren% a% ing from 1.1 V (× Li^+/Li) can be a×igned % %e red c%on po%en%al of LiTFA. The red c%on pecie× from TFA⁻, PF_6^-, or FEC in %e Li^+ ol a%on he a% can become po%on of SEI and affec% % prope% × (ion % an fer kine% ×, × rface energ , e%). In %e b lk elec%ol % of $LiPF_6$-EC/DEC (**Figure 5**a), %e Li^+ ol a%on he a% a× compo×ed of a gre% amo n% of EC, DEC molec le×, and li% PF_6^-. Once %e elec%o- chemical reac%on occ r×, %e EC, DEC molec le×, and PF_6^- in %e Li^+ ol a%on he a% ill be red ced b elec%on× and com- po×e %e main componen% of SEI. The SEI a× principall compo×ed of more organic componen% ($ROCO_2Li$) deri ed from EC or DEC ol en% di%ib %d in %e o %er la er, accom- panied b fe inorganic prod c% (Li_2O and LiF) in %e inner la er. Before depo×i%on, Li^+ had % o ercome large energ barri- er % break p %e Li^+ ol a%on he a%. When Li^+ %an po%d % %ro gh SEI, %e highl re i×%e organic $ROCO_2Li$ pecie× % large energ barrier blocked Li^+ diff ×ion and ind ced ne en charge di%ib %on, × b eq en% leading % dendri% Li gro %. Af%r replacing EC/DEC % DME/FEC (Fig re 5b), %e energ barrier of Li^+ de ol a%on had ligh% decrea×ed d e % eaker ol a%on of FEC compared % EC.[34] The Li^+ diff ×ion barrier acro× %e SEI al×o be red ced. Thi× can be a×cribed % %e increa×ed con%en% of LiF from FEC in addi%on % PF_6^- in %e SEI, hich enhanced %e %an po% kine% × of Li^+ and pro- d ced le× dendri% morpholog . In con%a% for LiTFA-DME/ FEC elec%ol % (Fig re 5c), TFA⁻ reg la%d %e en ironmen% of

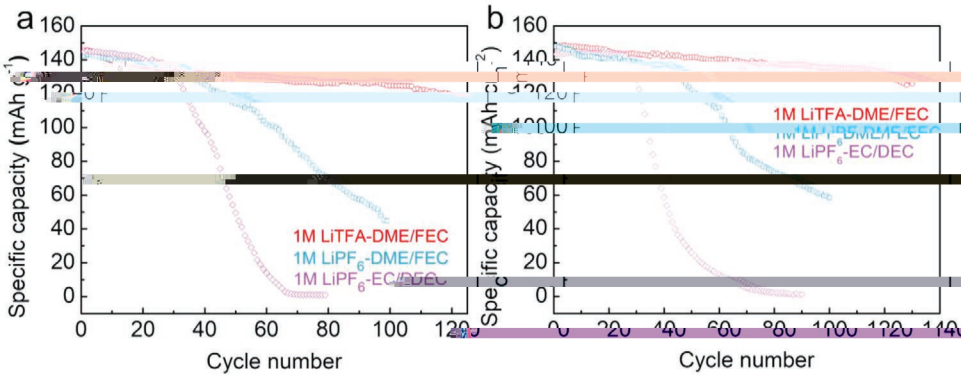

Figure 6. Electrochemical performances of Li metal anodes using LFP and NCM622 as cathode materials. a) Cycling stability of LFP||Li cells in different electrolytes when cycled at 0.5 C. b) Cycling stability of NCM622||Li cells in different electrolytes when cycled at 1 C.

Li$^+$ sol ation shea and facil ed fa de-sol ation kine . Addi nall , lo er energ of LUMO an sol en TFA$^-$ in he Li$^+$ sol ation shea a preferen all red ced form a SEI an ab ndance of LiF and Li_2O from o r inner la er. Hence, hen Li$^+$ an po d ro gh SEI, he componen (LiF and Li_2O) pla ed a igni can ole. LiF can pre en he elec on e change, prod ce niform diff ion eld gradien and afford niform Li$^+$.[35] Li_2O a demon ed be bene cial for bili ing he SEI lm.[36] A a re lt an ab ndance of LiF and Li_2O, more ion channel re ed in maller energ barrier for Li$^+$ ge ro gh. Fa and niform pa al di b on of Li$^+$ nall go niform depo on morpholog .

The o ida on bili of ario elec ol a e al d ia CV. A ho n in Fig re S16, S pporting Information, he anodic c rren an LiTFA-DME/FEC remained ble p 4.2 V, hich g aran ed can be ed LFP. LFP an areal capac of ≈1.5 mAh cm^{-2} and Li (≈2 ne e ce) ere con- c d a he cell. LFP||Li cell in he hree differen elec ol all e hibi d a a pla a 3.4 V Li$^+$/Li, deli ering an in al di charge capac of ≈142 mAh g^{-1} (Fig re S17, S pporting Information). A **Figure 6**a ho ed, he LFP||Li cell LiTFA-DME/FEC elec ol pre en he be c cling bili re ining 85% of he original re er ible capac fter 100 c cle , an a erage CE of 99.5% (Fig re S18, S pporting Information), in compari on <50% capac re n- on for $LiPF_6$-EC/DEC in 45 c cle Tho gh DME/FEC mi ga capac fading, he LFP||Li cell q ickl deca to <50% of he original capac fter 75 c cle The fa capac deca i a cribed he lo Li pla ing/ pping CE in $LiPF_6$-EC/DEC and $LiPF_6$-DME/FEC elec ol In addi on, he aggre i e $LiNi_{0.6}Co_{0.2}Mn_{0.2}O_2$ (NCM622) ca ode a al ed f ll cell A 1 C (160 mA g^{-1}), he cell deli - ered an in al di charge capac of ≈145 mAh g^{-1} in hree elec ol (Fig re S19, S pporting Information). A ho n in Fig re S20, S pporting Information, he cell ing $LiPF_6$-EC/DEC e hibi d an a erage CE of 98.1% in r 23 c cle Ho e er, be ond 23 c cle q ickl dropped <95%, accom- panied b a fa capac deca and ermina d c cling a fter 70 c cle (Fig re 6b). Tho gh DME/FEC impro ed he CE and mi ga d capac fading, $LiPF_6$-FEC/DME e perienced abr p capac drop a fter abo 40 c cle In compari on, he cell in LiTFA-DME/FEC re ined a ble CE of 98.6% o er 130 c cle before failing. The elec ochemical performance a mainl a cribed high Li pla ing/ pping ef cienc .

In hi d , ble Li me al high CE ha been achie ed b in od cing TFA he Li$^+$ sol ation shea and reg la ing he SEI fa ion an po kine Wi h ong coordina- on Li$^+$, TFA$^-$ can replace pa of sol en molec le form he sol ation shea c re, leading lo er energ barrier for Li$^+$ de-sol ation. Addi nall , d e lo er energ of LUMO han sol en in Li$^+$ sol ation shea, TFA$^-$ ha a preferen al red on prod ce a ble SEI an ab ndance of LiF and Li_2O. S ch SEI effec el red ce he energ barrier for Li$^+$ diff ion, con b ing lo er n clea on o erpo en al and fa er ion an fer kine A a re homogeneo Li$^+$ an po acro he in erface acco n for a niform Li$^+$ depo on and high c cling bili Thi ork no onl pro ide fre h in igh on reg la ing he rea of anion in he Li$^+$ sol ation shea manip la he in erface chemi and a er Li$^+$ depo- on beha ior , b al o pa e ne a on con c ing ble SEI for high-energ -den ma rial .

Experimental Section

Materials: CH_2Cl_2 and LFP materials were purchased from MACKLIN and used as received. EC, DEC, DME, FEC, LiTFA, LiTFSI, and $LiPF_6$ were purchased from Sigma-Aldrich.

Electrochemical Measurements: The Li||Cu cells were assembled or disassembled in an Ar-filled glove box with oxygen and water contents below 0.1 ppm. Coin cells of 2025 type were used as the Li||Cu, Li||Li symmetric, LFP||Li, and NCM||Li cells. For the Li||Cu cells, Li metal was used as the counter and reference electrodes while a Cu substrate was used as the working electrode. The cells were cycled in the voltage range −0.5 to 1.0 V (vs Li$^+$/Li) at current densities of 0.5 mA cm^{-2} with a fixed capacity of 1.0 mAh cm^{-2} by a LAND galvanostatic device. The CE is defined as charging capacity over discharging capacity. For LFP||Li and NCM||Li cells, Li pre-deposited on the Cu substrate at ≈3.0 mAh cm^{-2} was used as the anode. The LFP (≈1.5 mAh cm^{-2}) and NCM (≈1.1 mAh cm^{-2}) electrodes were prepared by casting a slurry mixture containing 85 wt% active material, 10 wt% Super P, and 5 wt% polyvinylidene fluoride binder (PVDF) in *N*-methyl-2-pyrrolidone onto a carbon-coated aluminum (Al) foil. Celgard 2500 polypropylene membranes were used as the separator for the Li||Cu, LFP||Li, and NCM||Li cells. Liquid electrolyte of 30 µL (1 M LiTFA-DME, 1 M LiTFA-DME/FEC, 1 M LiTFA-EC/DEC, 1 M $LiPF_6$-DME/FEC, 1 M $LiPF_6$-DME/EC, or 1 M $LiPF_6$-EC/DEC) was used for the coin cells.

The ratio of DME:FEC was set at 7:3 and 1:1 for EC:DEC by volume. CV and EIS measurements (10 mV, 10^5–10^0 Hz) were performed using a VSP-300 multichannel workstation.

Characterization: The Li deposited on the Cu substrate was protected by an Ar atmosphere in a homemade container to avoid contact with air during the transfer process before characterization. The morphologies of the samples were characterized by SEM (FEI Nova Nano-SEM 430, 10 kV). XPS analysis was performed using an ESCALAB 250 instrument with Al Kα radiation (15 kV, 150 W) under a pressure of 4×10^{-8} Pa. The ionic conductivity of the different electrolytes was measured by a FE30 at room temperature. All samples were rinsed with DME to remove residual electrolyte, then dried under vacuum. Surface-enhanced Raman scattering was performed using a Jobin Yvon Lab RAM HR800 with a 632.8 nm He–Ne laser. For the surface-enhanced Raman spectroscopy sample, a commercial silver (Ag) foil was immersed in a freshly prepared 12% HNO_3 solution for 5 s. A sponge-type surface with a high degree of roughness was thus created to enhance the signal. ATR-FTIR spectra were recorded on a Nicolet iS5 iD7 ATR spectrometer equipped with a diamond KBr beam splitter. An empty ATR cell blanketed with argon was used to collect the background spectrum.

Theoretical Calculations: The chemical structures, bond strengths, and molecular orbital energy levels of the selected solutes and solvents were calculated using the DFT method implemented in the Vienna ab initio simulation package,[37] based on the generalized gradient approximation of Perdew–Burke–Ernzerhof with a plane wave energy cutoff of 400 eV.[38]

Supporting Information

Supporting Information is available from the Wiley Online Library or from the author.

Acknowledgements

The authors thank Dr. Qinwei Wei and Dr. Xinxin Wei for the valuable discussions. They acknowledge financial support from National Natural Science Foundation of China (Grant Nos. 51525206, 51972312, 51472249, 51902316), Ministry of Science and Technology of the People's Republic of China (2016YFA0200100 and 2016YFB0100100), the Strategic Priority Research Program of the Chinese Academy of Sciences (XDA22010602), the Key Research Program of the Chinese Academy of Sciences (Grant No. KGZD-EW-T06), and the Bureau of Industry and Information Technology of Shenzhen for the "2017 Graphene Manufacturing Innovation Center Project" (Grant No. 201901171523). The theoretical calculations in this work were performed on TianHe-1(A) at National Supercomputer Center in Tianjing and Tianhe-2 at National Supercomputer Center in Guangzhou.

Conflict of Interest

The authors declare no conflict of interest.

Keywords

anions, energy barriers, lithium metal anodes, solid electrolyte interphase, solvation sheaths

Received: November 23, 2019
Revised: January 17, 2020
Published online:

[1] D. C. Lin, Y. Y. Liu, Y. Cui, *Nat. Nanotechnol.* **2017**, *12*, 194.
[2] D. Aurbach, E. Zinigrad, Y. Cohen, H. Teller, *Solid State Ionics* **2002**, *148*, 405.
[3] a) W. Xu, J. L. Wang, F. Ding, X. L. Chen, E. Nasybulin, Y. H. Zhang, J. G. Zhang, *Energy Environ. Sci.* **2014**, *7*, 513; b) X. Liang, Q. Pang, I. R. Kochetkov, M. S. Sempere, H. Huang, X. Q. Sun, L. F. Nazar, *Nat. Energy* **2017**, *2*, 17119; c) C. Z. Sun, A. Lin, W. W. Li, J. Jin, Y. Y. Sun, J. H. Yang, Z. Y. Wen, *Adv. Energy Mater.* **2019**, *10*, 1902989.
[4] a) X. Q. Zhang, X. Chen, X. B. Cheng, B. Q. Li, X. Shen, C. Yan, J. Q. Huang, Q. Zhang, *Angew. Chem., Int. Ed.* **2018**, *57*, 5301; b) J. Guo, Z. Y. Wen, M. F. Wu, J. Jin, Y. Liu, *Electrochem. Commun.* **2015**, *51*, 59.
[5] X. Q. Zhang, X. Chen, L. P. Hou, B. Q. Li, X. B. Cheng, J. Q. Huang, Q. Zhang, *ACS Energy Lett.* **2019**, *4*, 411.
[6] a) J. F. Qian, W. A. Henderson, W. Xu, P. Bhattacharya, M. Engelhard, O. Borodin, J. G. Zhang, *Nat. Commun.* **2015**, *6*, 6362; b) K. Xu, Y. F. Lam, S. S. Zhang, T. R. Jow, T. B. Curtis, *J. Phys. Chem. C* **2007**, *111*, 7411.
[7] Z. X. Wang, C. G. Sun, Y. Shi, F. L. Qi, Q. W. Wei, X. Li, Z. H. Sun, B. G. An, F. Li, *J. Power Sources* **2019**, *439*, 227073.
[8] R. Younesi, G. M. Veith, P. Johansson, K. Edström, T. Vegge, *Energy Environ. Sci.* **2015**, *8*, 1905.
[9] X. L. Fan, L. Chen, X. Ji, T. Deng, S. Hou, J. Chen, J. Zheng, F. Wang, J. J. Jiang, K. Xu, C. S. Wang, *Chem* **2018**, *4*, 174.
[10] X. L. Fan, L. Chen, O. Borodin, X. Ji, J. Chen, S. Hou, T. Deng, J. Zheng, C. Y. Yang, S. C. Liou, K. Amine, K. Xu, C. S. Wang, *Nat. Nanotechnol.* **2018**, *13*, 715.
[11] W. D. Zhang, S. Q. Zhang, L. Fan, L. N. Gao, X. Q. Kong, S. Y. Li, J. Li, X. Hong, Y. Y. Lu, *ACS Energy Lett.* **2019**, *4*, 644.
[12] a) Z. Q. Zhu, Y. X. Tang, Z. S. Lv, J. Q. Wei, Y. Y. Zhang, R. H. Wang, W. Zhang, H. R. Xia, M. Z. Ge, X. D. Chen, *Angew. Chem., Int. Ed.* **2018**, *57*, 3656; b) J. W. Meng, F. L. Chu, J. L. Hu, C. L. Li, *Adv. Funct. Mater.* **2019**, *29*, 1902220; c) J. L. Hu, K. Y. Chen, C. L. Li, *ACS Appl. Mater. Interfaces* **2018**, *10*, 34322.
[13] L. M. Suo, W. J. Xue, M. Gobet, S. G. Greenbaum, C. Wang, Y. M. Chen, W. L. Yang, Y. X. Li, J. Li, *Proc. Natl. Acad. Sci. USA* **2018**, *115*, 1156.
[14] J. M. Zheng, J. A. Lochala, A. Kwok, Z. D. Deng, J. Xiao, *Adv. Sci.* **2017**, *4*, 1700032.
[15] C. Yan, H. R. Li, X. Chen, X. Q. Zhang, X. B. Cheng, R. Xu, J. Q. Huang, Q. Zhang, *J. Am. Chem. Soc.* **2019**, *141*, 9422.
[16] H. Tokuda, S. I. Tabata, M. Susan, K. Hayamizu, M. Watanabe, *J. Phys. Chem. B* **2004**, *108*, 11995.
[17] D. M. Seo, S. Reininger, M. Kutcher, K. Redmond, W. B. Euler, B. L. Lucht, *J. Phys. Chem. C* **2015**, *119*, 14038.
[18] E. M. Erickson, E. Markevich, G. Salitra, D. Sharon, D. Hirshberg, E. de la Llave, I. Shterenberg, A. Rosenman, A. Frimer, D. Aurbach, *J. Electrochem. Soc.* **2015**, *162*, A2424.
[19] a) B. F. Li, J. Zhao, Z. H. Zhang, C. Zhao, P. F. Sun, P. X. Bai, J. X. Yang, Z. Zhou, Y. H. Xu, *Adv. Funct. Mater.* **2019**, *29*, 1807137; b) D. Xu, J. M. Su, J. Jin, C. Sun, Y. D. Ruan, C. H. Chen, Z. Y. Wen, *Adv. Energy Mater.* **2019**, *0*, 1900611.
[20] X. Q. Zhang, X. B. Cheng, X. Chen, C. Yan, Q. Zhang, *Adv. Funct. Mater.* **2017**, *27*, 1605989.
[21] K. K. Lee, K. Park, H. Lee, Y. Noh, D. Kossowska, K. Kwak, M. Cho, *Nat. Commun.* **2017**, *8*, 14658.
[22] a) L. D. Kock, M. D. S. Lekgoathi, P. L. Crouse, B. M. Vilakazi, *J. Mol. Struct.* **2012**, *1026*, 145; b) S. Sankarasubramanian, J. Kahky, V. Ramani, *Proc. Natl. Acad. Sci. USA* **2019**, *116*, 14899.
[23] Q. Zhao, Z. Y. Tu, S. Y. Wei, K. H. Zhang, S. Choudhury, X. T. Liu, L. A. Archer, *Angew. Chem., Int. Ed.* **2018**, *57*, 992.
[24] K. Xu, A. Von Cresce, U. Lee, *Langmuir* **2010**, *26*, 11538.
[25] Y. P. Guo, P. Niu, Y. Y. Liu, Y. Ouyang, D. Li, T. Y. Zhai, H. Q. Li, Y. Cui, *Adv. Mater.* **2019**, *31*, 1900342.
[26] K. Xu, *J. Electrochem. Soc.* **2007**, *154*, A162.
[27] X. Bogle, R. Vazquez, S. Greenbaum, A. v. W. Cresce, K. Xu, *J. Phys. Chem. Lett.* **2013**, *4*, 1664.

[28] X. Li, J. M. Zheng, M. H. Engelhard, D. H. Mei, Q. Y. Li, S. H. Jiao, N. Liu, W. G. Zhao, J. G. Zhang, W. Xu, *ACS Appl. Mater. Interfaces* **2018**, *10*, 2469.
[29] N. Togasaki, T. Momma, T. Osaka, *J. Power Sources* **2014**, *261*, 23.
[30] X. Shen, X. B. Cheng, P. Shi, J. Q. Huang, X. Q. Zhang, C. Yan, T. Li, Q. Zhang, *J. Energy Chem.* **2019**, *37*, 29.
[31] C. Yan, X. B. Cheng, Y. Tian, X. Chen, X. Q. Zhang, W. J. Li, J. Q. Huang, Q. Zhang, *Adv. Mater.* **2018**, *30*, 1707629.
[32] a) Y. Okuno, K. Ushirogata, K. Sodeyama, Y. Tateyama, *Phys. Chem. Chem. Phys.* **2016**, *18*, 8643; b) A. L. Michan, B. S. Parimalam, M. Leskes, R. N. Kerber, T. Yoon, C. P. Grey, B. L. Lucht, *Chem. Mater.* **2016**, *28*, 8149.
[33] J. Wang, Y. B. Yin, T. Liu, X. Y. Yang, Z. W. Chang, X. B. Zhang, *Nano Res.* **2018**, *11*, 3434.
[34] N. von Aspern, G. V. Röschenthaler, M. Winter, I. Cekic-Laskovic, *Angew. Chem., Int. Ed.* **2019**, *58*, 15978.
[35] a) Y. X. Yuan, F. Wu, Y. Bai, Y. Li, G. H. Chen, Z. H. Wang, C. Wu, *Energy Storage Mater.* **2019**, *16*, 411; b) Y. X. Yuan, F. Wu, G. H. Chen, Y. Bai, C. Wu, *J. Energy Chem.* **2019**, *37*, 197; c) S. Jurng, Z. L. Brown, J. Kim, B. L. Lucht, *Energy Environ. Sci.* **2018**, *11*, 2600.
[36] S. Q. Shi, P. Lu, Z. Y. Liu, Y. Qi, L. G. Hector, H. Li, S. J. Harris, *J. Am. Chem. Soc.* **2012**, *134*, 15476.
[37] G. Kresse, J. Furthmüller, *Phys. Rev. B* **1996**, *54*, 11169.
[38] J. P. Perdew, K. Burke, M. Ernzerhof, *Phys. Rev. Lett.* **1996**, *77*, 3865.